International Journal of Pharmaceutics 635 (2023) 122713

Contents lists available at ScienceDirect

International Journal of Pharmaceutics

journal homepage: www.elsevier.com/locate/ijpharm

Development of Thiol-Maleimide hydrogels incorporating graphene-based nanomaterials for cancer chemo-photothermal therapy

Francisco J.P. Costa [a], Micaela Nave [a], Rita Lima-Sousa [a], Cátia G. Alves [a], Bruna L. Melo [a], Ilídio J. Correia [a,b,*], Duarte de Melo-Diogo [a,*]

[a] CICS-UBI – Centro de Investigação em Ciências da Saúde, Universidade da Beira Interior, 6200-506 Covilhã, Portugal
[b] CIEPQPF – Departamento de Engenharia Química, Universidade de Coimbra, 3030-790 Coimbra, Portugal

ARTICLE INFO

Keywords:
Cancer
Chemo-photothermal therapy
Graphene family nanomaterials
Macroscale delivery systems
Thiol-Maleimide hydrogels

ABSTRACT

Nano-sized materials have been widely explored in the biomedicine field, especially due to their ability to encapsulate drugs intended to be delivered to cancer cells. However, systemically administered nanomaterials face several barriers that can hinder their tumor-homing capacity. In this way, researchers are now focusing their efforts in developing technologies that can deliver the nanoparticles directly into the tumor tissue. Particularly, hydrogels assembled using Thiol-Maleimide Michael type additions are emerging for this purpose due to their capacity to incorporate high nanoparticles' doses in a compact 3D structure as well as good chemical selectivity, biocompatibility, and straightforward preparation. Nevertheless, such hydrogels have been mostly prepared using synthetic polymers, which is not ideal due to their poor biodegradability. In this work, a novel natural polymer-based Thiol-Maleimide hydrogel was produced for application in breast cancer chemo-photothermal therapy. To obtain natural polymers compatible with this crosslinking chemistry, Hyaluronic acid was endowed with Thiol groups and deacetylated Chitosan was grafted with Maleimide groups. Parallelly, Doxorubicin loaded Dopamine-reduced graphene oxide (DOX/DOPA-rGO) was prepared for attaining Near Infrared (NIR) light responsive chemo-photothermal nanoagents. By simply mixing Hyaluronic Acid-Thiol, deacetylated Chitosan-Maleimide and DOX/DOPA-rGO, Thiol-Maleimide crosslinked hydrogels incorporating this nanomaterial could be assembled (DOX/DOPA-rGO@TMgel). When breast cancer cells were incubated with DOPA-rGO@TMgel and exposed to NIR light (photothermal therapy), their viability was reduced to about 59 %. On the other hand, DOX/DOPA-rGO@TMgel (chemotherapy) reduced cancer cells' viability to 50 %. In stark contrast, the combined action of DOX/DOPA-rGO@TMgel and NIR light decreased breast cancer cells' viability to just 21 %, highlighting its chemo-photothermal potential.

1. Introduction

Nanomaterials hold a great potential to improve cancer treatment due to their potential to reach the tumor zone by passive and/or active targeting mechanisms (Attia et al., 2019; Rosenblum et al., 2018). Furthermore, these nanostructures can incorporate active ingredients (*e.g.,* drugs, peptides) in their core, protecting them from premature degradation during blood circulation (Kumari et al., 2014; Mitchell

Abbreviations: ^{1}H NMR, Proton nuclear magnetic resonance; ANOVA, Analysis of variance; Ch, Chitosan; CLSM, Confocal Laser Scanning Microscopy; dCh-Mal, Maleimide-grafted deacetylated Chitosan; DLS, Dynamic Light Scattering; DMEM-F12, Dulbecco's Modified Eagle's Medium F-12; DOPA-rGO, Dopamine-reduced Graphene Oxide; DOPA-rGO@TMgel, Thiol-Maleimide HA-Ch based hydrogel incorporating DOPA-rGO; DOX, Doxorubicin; DOX/DOPA-rGO, Doxorubicin loaded DOPA-rGO; DOX/DOPA-rGO@TMgel, Thiol-Maleimide HA-Ch based hydrogel incorporating DOX/DOPA-rGO; EDC, 1-Ethyl-3-(3-dimethylaminopropyl) carbodiimide; EPR, Enhanced Permeability and Retention; FBS, Fetal Bovine Serum; FTIR, Fourier Transform Infrared; HA, Hyaluronic Acid; HA-Thiol, Thiol-grafted Hyaluronic acid; MCF-7, Michigan Cancer Foundation-7; NHDF, Normal Human Dermal Fibroblasts; NHS, *N*-Hydroxysuccinimide; NIR, Near Infrared; ns, Non-significant; PBS, Phosphate Buffered Saline; PI, Propidium Iodide; rGO, Reduced Graphene Oxide; S.D., Standard Deviation; SEM, Scanning Electron Microscopy; Sulfo-SMCC, 3-Sulfo-*N*-succinimidyl 4-(maleimidomethyl)-cyclohexane-1-carboxylate sodium salt; W/ NIR, With NIR laser exposure (808 nm, 1.7 W/cm^2); W/o NIR, Without NIR laser exposure.

* Corresponding authors at: CICS-UBI – Centro de Investigação em Ciências da Saúde, Universidade da Beira Interior, 6200-506 Covilhã, Portugal (I.J. Correia and D. de Melo-Diogo).

E-mail addresses: icorreia@ubi.pt (I.J. Correia), demelodiogo@fcsaude.ubi.pt (D. de Melo-Diogo).

https://doi.org/10.1016/j.ijpharm.2023.122713
Received 11 October 2022; Received in revised form 30 January 2023; Accepted 6 February 2023
Available online 9 February 2023

et al., 2021). As importantly, nanomaterials can be engineered to be responsive to a myriad of stimuli (*e.g.,* pH, light), opening the possibility to control the onset of the therapeutic effect (Mura et al., 2013; Zhang et al., 2022b).

Despite their potential, systemically administered nanomaterials face several barriers that hinder their full therapeutic capacity (Sriraman et al., 2014; Wilhelm et al., 2016). For instance, during circulation, nanomaterials can be covered by serum proteins, a phenomenon that alters their biodistribution (Sriraman et al., 2014; Wilhelm et al., 2016). Moreover, most nanomaterials are engineered to passively reach the tumor zone by taking advantage from the tumor's leaky vasculature (the so-called Enhanced Permeability and Retention (EPR) effect) (Alavi and Hamidi, 2019; Rosenblum et al., 2018). However, the EPR effect is overexaggerated in most pre-clinical models (*e.g.,* tumor-bearing mice), and it is not ubiquitously presented on human solid tumors (Dhaliwal and Zheng, 2019; Maeda, 2015). On the other hand, active targeting strategies, using nanomaterials decorated with ligands that bind to receptors overexpressed on cancer cells, is also a complex approach (Bertrand et al., 2014). This strategy is dependent on the receptor availability and a multitude of parameters related to the ligand (*e.g.,* density, spacer-arm length, shielding during circulation) (Pearce and O'Reilly, 2019; Zhang et al., 2020). These hurdles are further emphasized by the fact that <1 % of the systemically administered nanoparticles reach the tumor zone (Wilhelm et al., 2016).

In this way, researchers are now shifting their attention from systemic administration approaches to focus their efforts on developing technologies that can deliver the nanoparticles directly into the tumor tissue (local administration). In this context, macroscale systems (*e.g.,* hydrogels, microneedles, scaffolds) are emerging due to their capacity to sustain the nanomaterials' delivery into the tumor site (Kearney and Mooney, 2013; Moreira et al., 2019; Sun et al., 2020). Moreover, some of these macroscale systems can also be implanted after the surgical resection of the tumor, having an important role in eliminating any residual cancer cells and/or decreasing the likelihood of tumor's recurrence (Yang et al., 2021; Zhang et al., 2022a; Zhou et al., 2022).

Among the different implantable macroscale systems, hydrogels present a unique set of characteristics. Hydrogels have a straightforward formulation that only requires the usage of hydrophilic polymers and crosslinking agents (Bashir et al., 2020; Bustamante-Torres et al., 2021). Moreover, the hydrogels' hydrated polymer network acts as a giant reservoir that can accommodate nanomaterials as well as other therapeutic agents (Hoare and Kohane, 2008; Li and Mooney, 2016). Hydrogels can also be assembled with a well-defined architecture, which is important for postoperative strategies since it enables the filling of the resected tissue (Askari et al., 2020). For such purpose, chemically crosslinked hydrogels appear to be more advantageous due to their greater mechanical strength and high crosslinking degree, resulting in a compact 3D structure (Dimatteo et al., 2018; Parhi, 2017). In this regard, hydrogels assembled using Thiol-Maleimide Michael type additions offer a good chemical selectivity, biocompatibility, and do not require the use of initiators (that may be toxic) (Guaresti et al., 2019; Mather et al., 2006; Nair et al., 2014). However, such hydrogels have been mostly prepared using Poly(ethylene glycol) grafted with Thiol and/or Maleimide groups (Darling et al., 2016; Jansen et al., 2018; Shtenberg et al., 2017), which is not ideal considering the non-biodegradability of this synthetic polymer (Ewald et al., 2020; Wang et al., 2018).

In this work, a novel natural polymer-based Thiol-Maleimide implantable hydrogel was produced for application in the chemo-photothermal therapy of breast cancer cells. In order to attain natural polymers compatible with this crosslinking chemistry, Hyaluronic acid was modified with Cysteine (HA-Thiol) and deacetylated Chitosan was grafted with Sulfo-SMCC (dCh-Mal). Parallelly, Dopamine-reduced graphene oxide (DOPA-rGO) was produced since our team previously demonstrated its good photothermal capacity in response to Near Infrared (NIR; 750–1000 nm) light as well as its suitable cytocompatibility (Lima-Sousa et al., 2021). Then, DOPA-rGO was loaded with the chemotherapeutic drug Doxorubicin (DOX/DOPA-rGO) in order to attain a nanomaterial with chemo-photothermal capabilities.

By simply mixing HA-Thiol, dCh-Mal, and DOX/DOPA-rGO, Thiol-Maleimide crosslinked hydrogels incorporating this chemo-photothermal nanomaterial could be assembled (DOX/DOPA-rGO@TMgel). As control, Thiol-Maleimide hydrogels with only DOPA-rGO (*i.e.,* without DOX) were also produced (DOPA-rGO@TMgel). Both DOPA-rGO@TMgel and DOX/DOPA-rGO@TMgel presented a suitable gelation as well as a good porosity. Upon interaction with NIR radiation, these hydrogels could produce a temperature increase of approximately 22 °C, revealing a good photothermal capacity. In *in vitro* studies, the DOPA-rGO@TMgel revealed a good cytocompatibility. When breast cancer cells were incubated with DOPA-rGO@TMgel and exposed to NIR light (hydrogels' photothermal therapy), their viability reduced to about 59 %. On the other hand, DOX/DOPA-rGO@TMgel (hydrogels' chemotherapy) diminished cancer cells' viability to 50 %. In stark contrast, the combined action of DOX/DOPA-rGO@TMgel and NIR light decreased breast cancer cells' viability to just 21 %, highlighting its chemo-phototherapeutic potential.

2. Materials and methods

2.1. Materials

Chitosan (Ch; medium molecular weight), Graphene Oxide nanocolloids, *N*-Hydroxysuccinimide (NHS), Cysteine, Dulbecco's Modified Eagle's Medium F-12 (DMEM F-12), Resazurin, Phosphate Buffered Saline (PBS), Fetal Bovine Serum (FBS) and Penicillin/Streptomycin were acquired from Sigma-Aldrich (Sintra, Portugal).

3-Sulfo-*N*-succinimidyl 4-(maleimidomethyl)-cyclohexane-1-carboxylate sodium salt (Sulfo-SMCC), Propidium Iodide (PI) and Lysozyme from chicken egg were purchased from Alfa Aesar (Lancashire, UK). Methanol and T-flasks were bought from Thermo Fisher Scientific (Porto, Portugal). Dopamine hydrochloride was obtained from Acros Organics (New Jersey, USA). Calcein-AM was obtained from Merck Millipore (Algés, Portugal). NaOH was acquired from LabChem (Pennsylvania, USA). Doxorubicin (DOX) and Hyaluronic acid (HA; extra low molecular weight) were gotten from Carbosynth (Berkshire, UK). 1-Ethyl-3-(3-dimethylaminopropyl) carbodiimide (EDC) was obtained from Calbiochem (Darmstadt, Germany). Michigan Cancer Foundation-7 (MCF-7) cell line was provided by ATCC (Middlesex, UK). Normal Human Dermal Fibroblasts (NHDF) were supplied from PromoCell (Heidelberg, Germany). Cell culture plates were acquired from VWR (Alfragide, Portugal). The water used in the entire work was double deionized (0.22 μm filtered; 18.2 MΩ cm).

2.2. Methods

2.2.1. Synthesis and characterization of Maleimide-grafted deacetylated Chitosan and Thiol-grafted Hyaluronic acid

The production of Maleimide-grafted deacetylated Chitosan (dCh-Mal) was performed using a two-step process based on the deacetylation of Ch and its subsequent reaction with Sulfo-SMCC. Initially, the deacetylation of Ch was accomplished as previously described by our group with minor modifications (Gaspar et al., 2010). In brief, Ch (1 g) was mixed with NaOH (2 M; 20 mL) and it was allowed to react for 3 h at 50 °C under stirring. Then, this solution was washed with water, vacuum filtered and freeze-dried, yielding deacetylated Chitosan (dCh). Subsequently, Sulfo-SMCC was reacted with dCh according to the protocol described by El-Sayed *et al.* with minor modifications (El-Sayed et al., 2016). In brief, dCh (100 mg) and Sulfo-SMCC (2.44 mg) were dissolved in PBS at pH 7.5 (10 mL). This mixture was left to react for 24 h under stirring at room temperature. The obtained product was then dialyzed against water for 3 days (14 kDa molecular weight cut-off membrane) and freeze-dried, yielding Maleimide-grafted deacetylated Chitosan

(dCh-Mal).

The synthesis of Thiol-grafted Hyaluronic acid (HA-Thiol) was performed as described previously by Sousa *et al.* (Pereira de Sousa et al., 2016), with minor adaptations. Briefly, an aqueous solution of HA (100 mg; 15 mL), EDC (466 mg; 5 mL) and NHS (92 mg; 3 mL) was prepared. The resultant solution pH was then adjusted to 5.5, and subsequently left to react for 30 min under stirring at room temperature. Afterwards, an aqueous solution of Cysteine (31.6 mg; 2 mL) was added to the previous mixture, being left to react for 4 h under stirring at room temperature. Finally, the final solution was dialyzed against water for 3 days (14 kDa molecular weight cut-off membrane) and freeze-dried, yielding Thiol-grafted Hyaluronic acid (HA-Thiol).

The successful synthesis of dCh, dCh-Mal and HA-Thiol were confirmed by Fourier-Transform Infrared (FTIR) spectroscopy, using a Nicolet iS10 spectrometer (ThermoScientific Inc., MA, USA). These polymers were also characterized by Proton Nuclear Magnetic Resonance (^{1}H NMR) using a Brüker Avance III 400 MHz spectrometer (Brüker Scientific Inc., NY, USA). For this purpose, dCh (30:1 (v/v) D_2O/HCl 1 M), dCh-Mal (30:1 (v/v) D_2O/HCl 1 M), HA (9:1 (v/v) H_2O/D_2O), Cysteine (9:1 (v/v) H_2O/D_2O), and HA-Thiol (9:1 (v/v) H_2O/D_2O) were analyzed at 298 K. The spectra obtained were analyzed in MestReNova software (Mestrelab Research, SL, Santiago de Compostela, Spain).

2.2.2. Formulation and characterization of the Thiol-Maleimide HA-Ch based hydrogels

The assembly of Thiol-Maleimide HA-Ch implantable hydrogels incorporating DOX/DOPA-rGO was performed according to the protocol by Matsumoto *et al.* with minor modifications (Matsumoto et al., 2016). The preparation and characterization of DOX/DOPA-rGO are described in the Supplementary Information. Briefly, aqueous solutions of DOX/DOPA-rGO (150 μL; 500 μg/mL of DOPA-rGO equivalents), HA-Thiol (50 μL; 40 mg/mL) and dCh-Mal (50 μL; 10 mg/mL) were mixed in round-bottom microtubes for attaining hydrogels with similar macroscopic properties for all the assays – abbreviated as DOX/DOPA-rGO@TMgel. After complete crosslinking, the formulations were recovered by gentle centrifugation and stored at 4 °C before their use. The supernatants were collected for determining the DOX incorporation efficiency in the hydrogel by fluorescence spectroscopy (λ_{ex} = 488 nm, λ_{em} = 590 nm; Spectramax Gemini EM spectrofluorometer, Molecular Devices LLC, USA) (Mó et al., 2020). For the formulation of the Thiol-Maleimide HA-Ch based hydrogels incorporating DOPA-rGO (abbreviated as DOPA-rGO@TMgel), the same protocol was employed using DOPA-rGO (150 μL; 500 μg/mL). As control, formulations i) without Maleimide groups (*i.e.*, prepared using dCh, HA-Thiol and DOPA-rGO) and ii) without Thiol groups (*i.e.,* prepared using dCh-Mal, HA and DOPA-rGO) were also produced.

The gelation of the produced hydrogels was confirmed by the inverted microtube method (Lima-Sousa et al., 2020). The superficial and inner (cross-section) morphologies of the hydrogels were observed by Scanning Electron Microscopy (SEM) operated at an acceleration voltage of 20 kV (Hitachi S-3400 N Scanning Electron Microscope, Japan). To visualize the degradation of the DOX/DOPA-rGO@TMgel and DOPA-rGO@TMgel in physiological-like conditions, these were immersed in PBS (pH 7.4) supplemented with Lysozyme (13.6 mg/L) and incubated at 37 °C under stirring for 7 days. Then, the hydrogels were recovered, washed with water, freeze-dried, and imaged by SEM as described above.

The rheological analysis of the pre-assembled hydrogels was performed in a Thermostated Brookfield DV3T cone-plate Rheometer utilizing a CP52Z cone (Brookfield Ametek, Massachusetts, USA). The apparent viscosity was assessed with increasing shear rates (40–500 1/s) as well as a function of time (15 s intervals, 30 min of total time, constant speed of 60 RPM). The assays were performed at 37 °C, and data with torque values superior to 95 % or inferior to 5 % were not considered for analysis.

To assess the long-term stability of the hydrogels, all the individual precursor solutions (*i.e.,* those containing dCh-Mal, HA-Thiol, DOPA-rGO or DOX/DOPA-rGO) were prepared and stored at 4 °C for 7 days. Afterwards, these aged precursor solutions were used to assemble the hydrogels, and their gelation was confirmed by the inverted microtube test. Additionally, DOPA-rGO and DOX/DOPA-rGO size distribution and NIR absorption after storage (for 7 days at 4 °C) were also assessed.

The photothermal capacity of DOX/DOPA-rGO@TMgel and DOPA-rGO@TMgel was investigated as previously described by us (Lima-Sousa et al., 2018). In brief, these formulations were placed in water and irradiated with NIR light (808 nm, 1.7 W/cm^2) for 10 min. The temperature variations (ΔT) were recorded by using a thermocouple thermometer. As a control, the temperature change of water (without hydrogels) was also measured.

2.2.3. In vitro evaluation of the cytocompatibility of the DOPA-rGO@TMgel

To evaluate the cytocompatibility of DOPA-rGO@TMgel, this formulation was placed in contact with models of healthy (NHDF) and breast cancer (MCF-7) cells (Lima-Sousa et al., 2020). Briefly, a density of 2 × 10^4 cells/well was seeded in 24-well plates in DMEM F-12 medium supplemented with 10 % FBS and 1 % Penicillin/streptomycin and cultured in a humidified incubator (at 37 °C; 5 % CO_2). After 24 h of cells' growth, these were incubated with fresh culture medium (0.5 mL/well) containing DOPA-rGO@TMgel (at 150 μg/mL of DOPA-rGO) and DOPA-rGO (at 75 or 150 μg/mL) for 24 h and 48 h. Afterwards, the formulations were removed from the wells, the medium was replaced with fresh medium containing resazurin (10 % (v/v)) and the cells were incubated for 4 h in the dark (at 37 °C; 5 % CO_2). Cell viability was assessed after the incubation period by reading the fluorescence of the Resorufin (λ_{ex} = 560 nm, λ_{em} = 590 nm) in a Spectramax Gemini EM spectrofluorometer (Molecular Devices LLC, USA) (Sabino et al., 2021). In addition, cells were also incubated with only culture medium or ethanol (70 % (v/v)), being the negative (K-) or positive (K +) controls, respectively.

2.2.4. In vitro evaluation of the photothermal therapy mediated by DOPA-rGO@TMgel and chemo-photothermal therapy mediated by DOX/DOPA-rGO@TMgel

The DOPA-rGO@TMgel' and DOX/DOPA-rGO@TMgel' photo-therapeutic potential against breast cancer cells was assessed using the resazurin method (Lima-Sousa et al., 2020). For such, the same cell density of MCF-7 cells described in 2.2.3. was cultured and, after 24 h, these were incubated with fresh culture medium (0.5 mL/well) containing DOPA-rGO@TMgel (150 μg/mL of DOPA-rGO), DOX/DOPA-rGO@TMgel (0.44 μg/mL of DOX; 150 μg/mL of DOPA-rGO), DOX/DOPA-rGO (0.44 μg/mL of DOX; 150 μg/mL of DOPA-rGO) and DOX (0.44 μg/mL). Four hours later, the hydrogels were exposed to NIR light (808 nm, 1.7 W/cm^2) for 10 min. Upon reaching 24 h of incubation with the formulations, the cells were incubated with resazurin, and their viability was determined as described in Section 2.2.3.

In order to obtain visual confirmation of the therapeutic effect of DOPA-rGO@TMgel and DOX/DOPA-rGO@TMgel, MCF-7 cells were first seeded and incubated with these formulations as described above (Lima-Sousa et al., 2020). After 4 h, the hydrogels were irradiated with NIR light (808 nm, 1.7 W/cm^2, 10 min), and the cells were stained with Calcein-AM/PI (used to label live/dead cells, respectively) according to the manufacturer's protocol. Fluorescence images were acquired by Confocal Laser Scanning Microscopy (CLSM; Zeiss LSM 710, Carl Zeiss AG, Oberkochen, Germany) using a $\lambda_{ex}/\lambda_{em}$ of 488/493–556 (Calcein-AM) and 561/566–719 nm (PI) (Melo et al., 2021). Non-irradiated cells exclusively incubated with culture medium were considered the control for live cells.

2.2.5. Statistical analysis

For multiple groups comparison, a one-way Analysis of Variance (ANOVA) was applied with the Student-Newman-Keuls test. A *p*-value

lower than 0.05 ($p < 0.05$) was deemed statistically significant. All data are represented as the mean ± standard deviation (S.D.). Data analysis was achieved using the software GraphPad Prism v6.0 (Trial version, GraphPad Software, CA, USA).

3. Results and discussion

3.1. Formulation and characterization of the Thiol-Maleimide HA-Ch based hydrogels

To prepare the Thiol-Maleimide implantable hydrogels, initially Maleimide-grafted deacetylated Chitosan (dCh-Mal) and Thiol-grafted Hyaluronic acid (HA-Thiol) were synthesized and characterized by FTIR and ^{1}H NMR (Supplementary Information: Figs. S1–S3). Parallelly, DOPA-rGO was prepared as previously described by our group (Lima-Sousa et al., 2021), being then loaded with DOX and characterized (Supplementary Information: Fig. S4).

Then, aqueous solutions containing HA-Thiol, dCh-Mal and DOX/DOPA-rGO were mixed, leading to the assembly of the Thiol-Maleimide hydrogels incorporating this nanomaterial – termed as DOX/DOPA-rGO@TMgel (Fig. 1A). The incorporation efficiency of DOX in DOX/DOPA-rGO@TMgel was approximately 99 % (n = 3). The same procedure was also applied using DOPA-rGO, leading to the assembly of DOPA-rGO@TMgel. After the mixing and reaction processes (≈ 45–90 min), the gelation of the hydrogels was confirmed by the inverted microtube test (Fig. 1B1-2 and C1-2). As control, formulations without Maleimide groups (*i.e.,* prepared using dCh, HA-Thiol and DOPA-rGO) and without Thiol groups (*i.e.,* prepared using dCh-Mal, HA and DOPA-rGO) were also prepared – Fig. S5. The formulations without Maleimide groups remained as a solution and did not achieve gelation

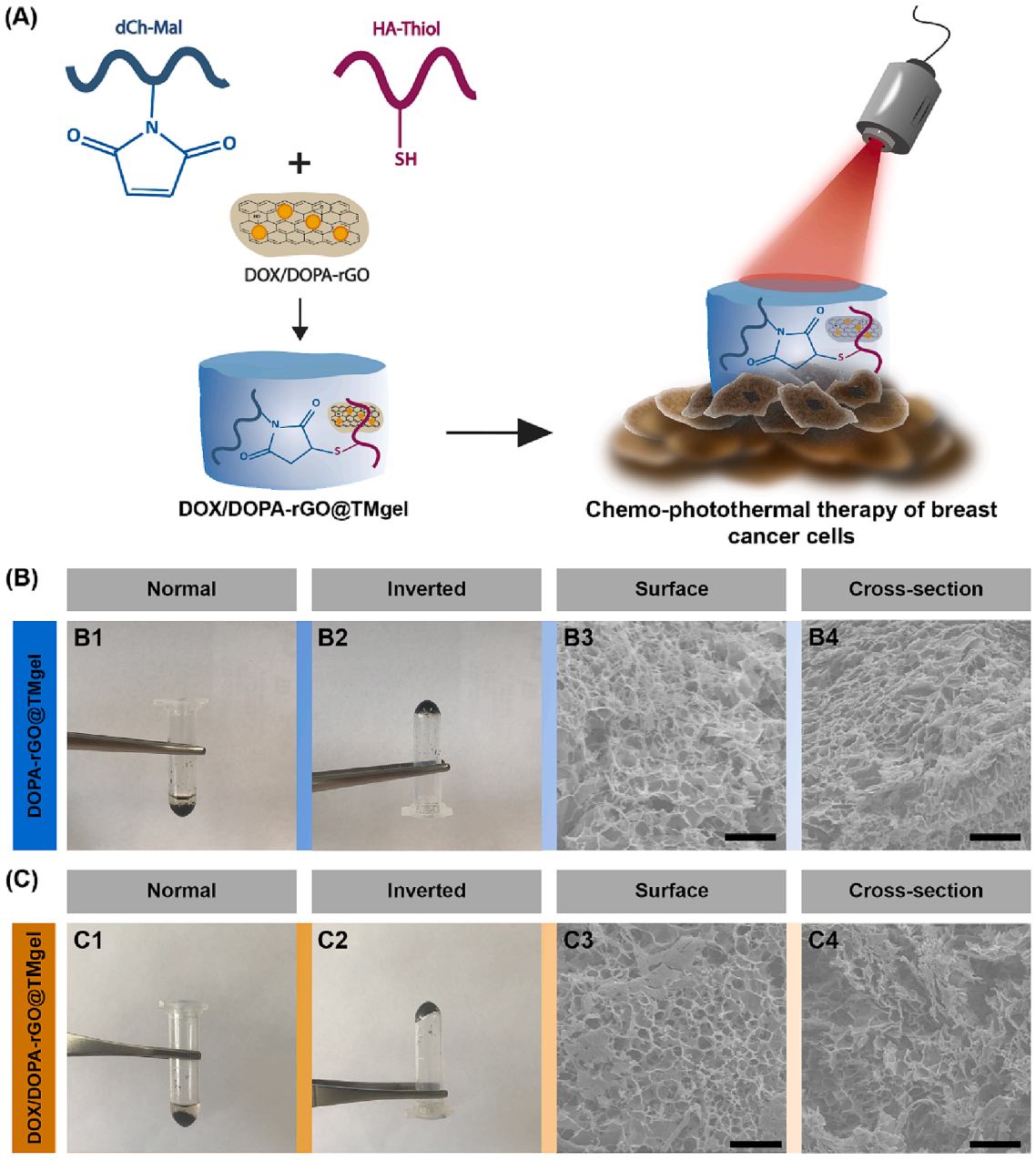

Fig. 1. Illustration of the formulation of the Thiol-Maleimide based implantable hydrogel incorporating DOX/DOPA-rGO, and its use in the chemo-photothermal therapy of breast cancer cells (A). Macroscopic images of the gelation of the DOPA-rGO@TMgel (B1-2) and DOX/DOPA-rGO@TMgel (C1-2) assessed by the inverted microtube test. SEM images of the surface and cross-section of DOPA-rGO@TMgel (B3-4) and DOX/DOPA-rGO@TMgel (C3-4). Scale bars represent 100 μm.

(Fig. S5A). The formulation prepared without Thiol groups appeared to precipitate, but no gelation was observed (Fig. S5B). Together, these results corroborate that the Thiol-Maleimide Michael type addition reaction between the HA-Thiol and dCh-Mal is crucial for the assembly of the DOPA-rGO@TMgel and DOX/DOPA-rGO@TMgel.

Subsequently, the morphology and porosity of the produced hydrogels were assessed by imaging their surface and interior (cross-section) by SEM (Fig. 1B3-4 and C3-4). The DOPA-rGO@TMgel and DOX/DOPA-rGO@TMgel displayed a uniform porous structure at their surface (Fig. 1B3 and C3) and interior (Fig. 1B4–C4), which is crucial for nanomaterials' diffusion (Ganguly and Margel, 2021). Moreover, the formulations' pores appeared to be highly interconnected, which is a characteristic of densely packed hydrogels such as those that are chemically crosslinked (Liu et al., 2016; Xie et al., 2021). The rheological analysis demonstrated that the viscosity of both DOPA-rGO@TMgel and DOX/DOPA-rGO@TMgel decreases with the increase in the applied shear rate, suggesting a shear-thinning behavior (non-Newtonian) (Fig. 2A) (Mondal et al., 2019; Olaru et al., 2018). In turn, when the viscosity of the pre-assembled hydrogels was analyzed as a function of time (fixed speed), the obtained values were constant (Fig. S6). Such data also confirms the successful gelation of the produced hydrogels (Lupu et al., 2023).

Furthermore, the degradability of DOPA-rGO@TMgel and DOX/DOPA-rGO@TMgel, under conditions similar to the human physiological environment, was visualized by SEM (Fig. 3). The images revealed an incubation-time dependent degradation of the polymeric network, both on the hydrogels' surface (Fig. 3A-C) and interior (Fig. 3D–F). This behavior is in line with the excellent biodegradability of Ch- and HA-based hydrogels (Ahmadi et al., 2015; Park et al., 2019; Shariatinia and Jalali, 2018; Trombino et al., 2019). As importantly, it could be fundamental to allow the diffusion of the entrapped agents as well as eliminate the need to remove the hydrogels (by surgery) after their therapeutic effect (Ozcelik, 2016; Sheth et al., 2019).

Afterwards, the long-term stability of the hydrogel precursor solutions was investigated (Figs. S7 and S8). For this purpose, the aqueous solutions containing the individual polymers (HA-Thiol and dCh-Mal) and the therapeutic agents (DOPA-rGO or DOX/DOPA-rGO) were stored at 4 °C for a total of 7 days. As it can be seen in Figure S7 and S8, both DOPA-rGO and DOX/DOPA-rGO maintained their size distribution (Figs. S7A and S8A) and NIR absorbance (Figs. S7B and S8B). Such is crucial to ensure that these nanomaterials retain their therapeutic potential (related to their size and photothermal capacity) even after prolonged storage. As importantly, when all the aged/stored solutions were mixed, the DOPA-rGO@TMgel and DOX/DOPA-rGO@TMgel gelified in a similar manner (Figs. S7C and S8C), indicating that their ability to form Thiol-Maleimide bonds is retained.

Then, the photothermal capacity of DOPA-rGO@TMgel and DOX/DOPA-rGO@TMgel was studied by irradiating them with NIR light (808 nm, 1.7 W/cm^2) for 10 min, and measuring the attained temperature variations (ΔT) – Fig. 2B. As expected, the photoinduced heat generated by both formulations was dependent on the irradiation time (Figs. 2B and S9). After 10 min of NIR laser exposure, both DOPA-rGO@TMgel and DOX/DOPA-rGO@TMgel produced a similar temperature increase of 21–22 °C (ΔT), which can be explored to induce damage on cancer cells (Huang et al., 2006). A control test using water exposed to NIR light showed a minimal temperature increase, which is in line with the low interaction of water with this radiation (Shanmugam et al., 2014).

In a recent work, Wu *et al.* created a methylcellulose-based hydrogel incorporating IR820 (500 μg/mL), which mediated a temperature increase of about 29 °C upon NIR irradiation (808 nm, 2 W/cm^2, 5 min) (Wu et al., 2021). Melo *et. al.* produced a Ch-$NaHCO_3$ based hydrogel that also contained DOPA-rGO (66.7 μg/mL), which produced a photoinduced heat of about 12 °C upon NIR laser exposure (808 nm, 1.7 W/cm^2, 10 min) (Melo et al., 2022). Herein, the DOPA-rGO@TMgel and DOX/DOPA-rGO@TMgel (150 μg/mL of DOPA-rGO) could generate a temperature increase of about 21–22 °C upon laser exposure (808 nm, 1.7 W/cm^2, 10 min), demonstrating their good photothermal potential.

3.2. *In vitro evaluation of the cytocompatibility of the DOPA-rGO@TMgel*

After confirming the photothermal capacity of the hydrogels, the cytocompatibility profile of DOPA-rGO@TMgel (at 150 μg/mL of DOPA-rGO) in healthy (NHDF) and breast cancer (MCF-7) cells was assessed (Fig. 4). Even after 48 h of incubation with this formulation, NHDF and MCF-7 cells remained with a viability of 70 and 90 %, respectively (Fig. 4). For comparison purposes, both cell lines were also incubated directly with DOPA-rGO (Fig. S10). In agreement with our previous work (Lima-Sousa et al., 2021), the DOPA-rGO, at the concentration of 75 μg/mL, did not affect meaningfully these cell lines (viability > 76 %) – Fig. S10. However, increasing the dose of DOPA-rGO to 150 μg/mL led to a decrease on the cells' viability to about 39 % (Fig. S10). Considering that the DOPA-rGO@TMgel also contains this same DOPA-rGO dose, this data suggests that the incorporation of this nanomaterial in the developed hydrogels is crucial to enhance its cytocompatibility.

In fact, the good cytocompatibility of DOPA-rGO@TMgel may be related to the use of biocompatible polymers (HA and Ch) in its

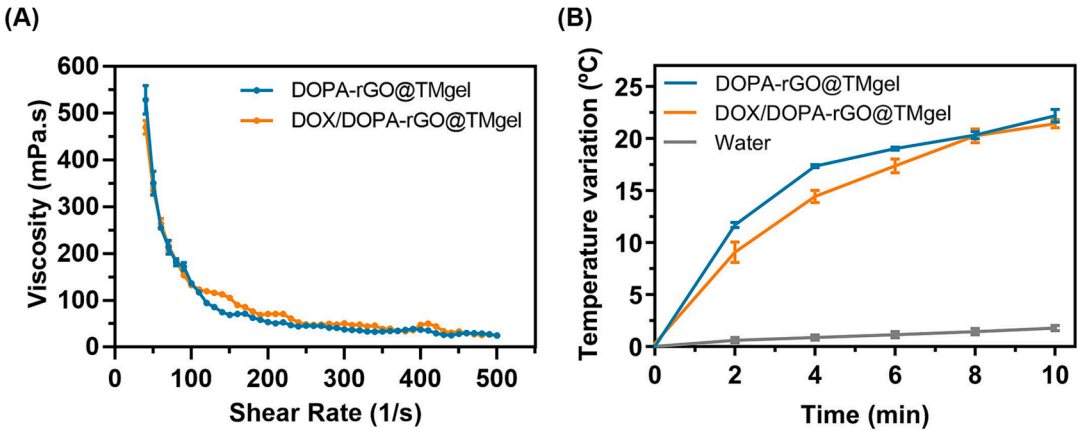

Fig. 2. Apparent viscosity of DOPA-rGO@TMgel and DOX/DOPA-rGO@TMgel at different increasing shear rates (40–500 1/s) (A). Temperature variation curves of DOPA-rGO@TMgel, DOX/DOPA-rGO@TMgel and water upon irradiation with NIR light (808 nm, 1.7 W/cm^2) during 10 min (B). Data represents mean ± S.D., n = 3.

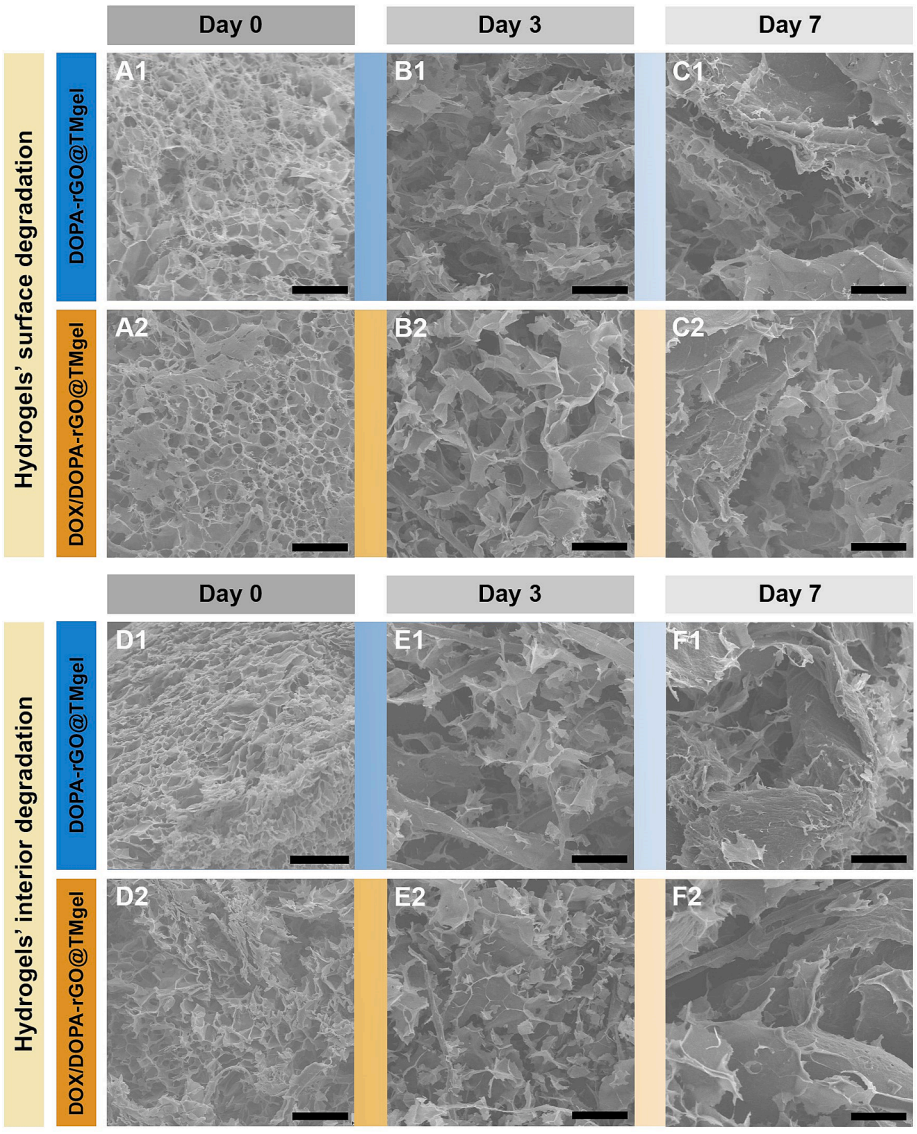

Fig. 3. SEM images of DOPA-rGO@TMgel and DOX/DOPA-rGO@TMgel surface after 0 (A1, A2), 3 (B1, B2) and 7 (C1, C2) days of incubation in PBS (pH 7.4) supplemented with Lysozyme. SEM images of DOPA-rGO@TMgel and DOX/DOPA-rGO@TMgel interior (cross-section) after 0 (D1, D2), 3 (E1, E2) and 7 (F1, F2) days of incubation in the same conditions. Scale bar indicates 100 μm.

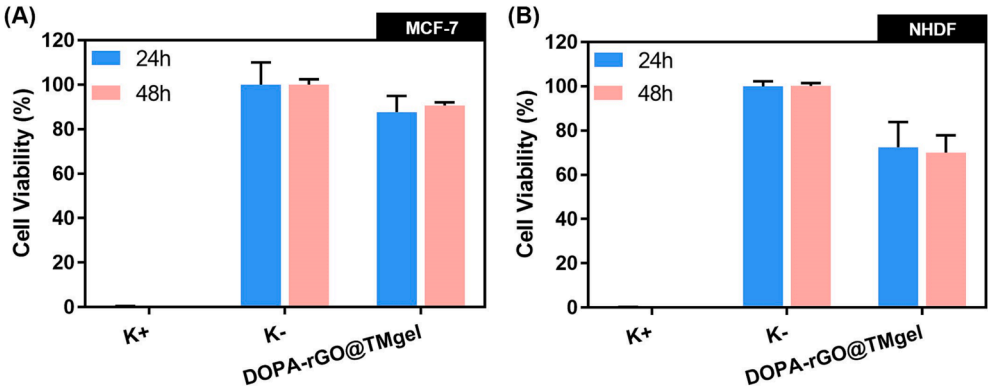

Fig. 4. Viability of MCF-7 cells (A) and NHDF (B) after 24 and 48 h of incubation with DOPA-rGO@TMgel. Data represents mean ± S.D., n = 5. K− represents the negative control and K+ represents the positive control.

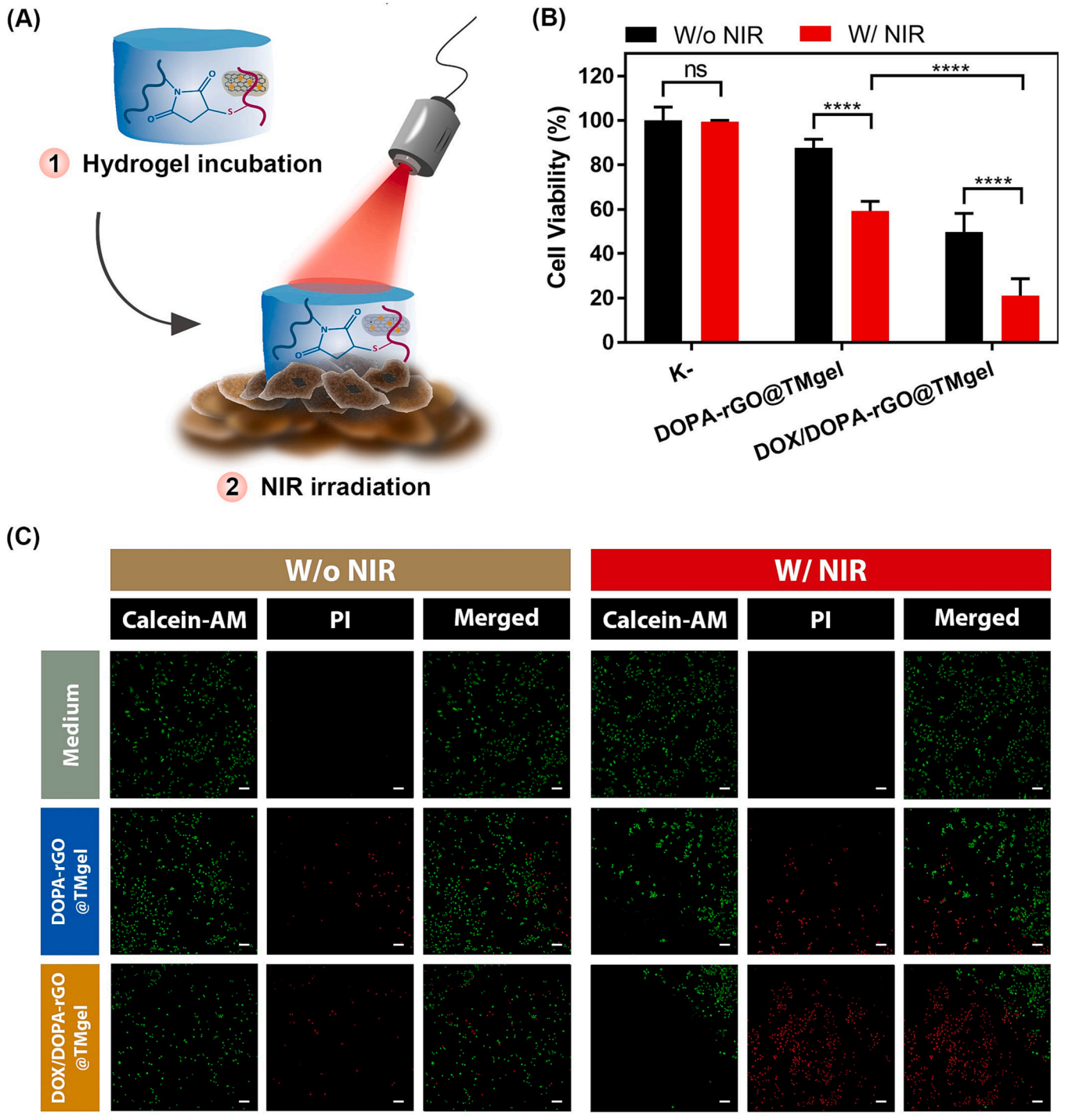

Fig. 5. Schematic depicting the chemo-photothermal therapy mediated by DOX/DOPA-rGO@TMgel (A). Therapeutic effect of DOPA-rGO@TMgel (150 μg/mL of DOPA-rGO) and DOX/DOPA-rGO@TMgel (0.44 μg/mL of DOX; 150 μg/mL of DOPA-rGO) towards MCF-7 cells without (W/o NIR) and with (W/ NIR) NIR laser irradiation (808 nm, 1.7 W/cm^2, 10 min) (B). Data represents mean ± S.D., n = 5, ****$p < 0.0001$, ns = non-significant. K- W/o NIR represents the negative control and K- W/ NIR represents cells solely exposed to NIR light. CLSM images of MCF-7 cells stained with Calcein-AM/PI after incubation with DOPA-rGO@TMgel (150 μg/mL of DOPA-rGO) or DOX/DOPA-rGO@TMgel (0.44 μg/mL of DOX; 150 μg/mL of DOPA-rGO) W/o NIR or W/ NIR laser irradiation (808 nm, 1.7 W/cm^2, 10 min) (C). Medium W/o NIR represents the control for live cells, while Medium W/ NIR represents cells only exposed to NIR light. Green channel: Calcein-AM; red channel: PI. Scale bars correspond to 100 μm. (For interpretation of the references to colour in this figure legend, the reader is referred to the web version of this article.)

composition (Hamilton et al., 2021; Seo et al., 2021). Lima-Sousa *et al.* developed a Ch and Agarose based hydrogel incorporating rGO (reduced using Vitamin C) that also revealed a good cytocompatibility profile (Lima-Sousa et al., 2020). Other Ch and HA-based hydrogels reported in the literature also displayed good biological properties (Deng et al., 2017; Hu et al., 2021; Melo et al., 2022). Taken together, these results also indicate that the Thiol and Maleimide modifications were not detrimental for the hydrogels' biological properties, highlighting the hydrogels' suitability for cancer therapy.

3.3. In vitro evaluation of the photothermal therapy mediated by DOPA-rGO@TMgel and chemo-photothermal therapy mediated by DOX/DOPA-rGO@TMgel

By last, the phototherapeutic and chemo-phototherapeutic effects mediated by DOPA-rGO@TMgel (150 μg/mL of DOPA-rGO) and DOX/DOPA-rGO@TMgel (0.44 μg/mL of DOX; 150 μg/mL of DOPA-rGO), respectively, were assessed on MCF-7 cells. For this assay, the formulations were incubated with the breast cancer cells and then irradiated with NIR light for 10 min (808 nm, 1.7 W/cm^2) – Fig. 5A. For comparison purposes, these cells were also exposed directly to free DOX (0.44 μg/mL) and DOX/DOPA-rGO (0.44 μg/mL of DOX; 150 μg/mL of DOPA-rGO).

As expected, the single use of NIR irradiation did not affect MCF-7 cells' viability (≈ 99 %), which is in line with the scarce temperature variation that is attained when water is exposed to NIR light (Figs. 5B and 2B). On the other hand, when DOPA-rGO@TMgel was combined with NIR light (hydrogels' photothermal therapy), the breast cancer cells' viability showed a moderate decrease to 59 %. Closely, DOX/DOPA-rGO@TMgel (hydrogels' chemotherapy) only reduced the cells' viability to about 50 %. As expected, the action of free DOX (classic chemotherapy) also impacted cells by reducing their viability to about 53 %, while DOX/DOPA-rGO (nanomaterials' chemotherapy) diminished the cells' viability to about 33 % (Fig. S11). Interestingly, the combined action of DOX/DOPA-rGO@TMgel and NIR light (hydrogels' chemo-photothermal therapy) was able to reduce the breast cancer cells' viability to just 21 %. Among all the tested formulations, the DOX/DOPA-rGO@TMgel provided the best control over the therapeutic outcome since it induced a moderate toxicity towards breast cancer cells (viability ≈ 50 %), being this effect further boosted by ≈ 2.4-times upon NIR laser exposure (viability ≈ 21 %).

To confirm these results, breast cancer cells were also stained with Calcein-AM (labels live cells) and PI (labels dead cells) and imaged by CLSM (Fig. 5C). In concomitance with the cell viability results, cells exposed to just NIR light only displayed Calcein-AM fluorescence signals. In turn, the breast cancer cell populations exposed to DOPA-rGO@TMgel plus NIR light (hydrogels' photothermal therapy) and DOX/DOPA-rGO@TMgel (hydrogels' chemotherapy) presented both Calcein-AM and PI fluorescence signals, indicating that these cells are only partially eliminated. In stark contrast, the majority of the breast cancer cells incubated with DOX/DOPA-rGO@TMgel plus NIR light revealed PI fluorescence signals, further confirming the enhanced therapeutic outcome arising from the hydrogels' chemo-photothermal therapy.

For instance, He *et al.* prepared a polypeptide based hydrogel containing black phosphorus nanosheets (400 μg/mL; photothermal agent) and Bufalin (50 nmol/L; chemotherapeutic agent) that, upon NIR irradiation (808 nm, 1.0 W/cm^2, 10 min), could decrease colon cancer cells' viability to about 27 % (He et al., 2021). In another work, Melo *et al.* produced an Ch-$NaHCO_3$ based hydrogel that incorporated DOPA-rGO (66.7 μg/mL) and Resveratrol (35 μg/mL), which upon NIR laser exposure (808 nm, 1.7 W/cm^2, 10 min), diminished the viability of breast cancer cells to about 31 % (Melo et al., 2022). Herein, the DOX/DOPA-rGO@TMgel (0.44 μg/mL of DOX; 150 μg/mL of DOPA-rGO) combined with NIR light (808 nm, 1.7 W/cm^2, 10 min) reduced the breast cancer cells' viability to just 21 %, highlighting its potential for chemo-photothermal therapy.

4. Conclusion

In this work, DOX/DOPA-rGO@TMgel was prepared, for the first time, for application in cancer chemo-photothermal therapy. The preparation of this hydrogel revealed to be a simple process since it only relied on the mixing of dCh-Mal, HA-Thiol and DOX/DOPA-rGO. For comparison purposes, DOPA-rGO@TMgel was also assembled. Both DOPA-rGO@TMgel and DOX/DOPA-rGO@TMgel presented a suitable gelation as well as a good porosity. Upon interaction with NIR radiation, these hydrogels could produce a temperature increase of approximately 22 °C, revealing a good photothermal capacity. In *in vitro* studies, the DOPA-rGO@TMgel revealed a good cytocompatibility towards both healthy and breast cancer cells. When breast cancer cells were incubated with DOPA-rGO@TMgel and exposed to NIR light (hydrogels' photothermal therapy), their viability reduced to about 59 %. On the other hand, DOX/DOPA-rGO@TMgel (hydrogels' chemotherapy) reduced cancer cells' viability to 50 %. In stark contrast, the combined action of DOX/DOPA-rGO@TMgel and NIR light decreased breast cancer cells' viability to just 21 %, highlighting its chemo-phototherapeutic potential. In the future, evaluating the long-term biocompatibility of DOPA-rGO@TMgel as well as the efficacy of the implantable DOX/DOPA-rGO@TMgel in postoperative chemo-photothermal therapy (at the current and lower NIR laser intensities) will give an important insight about its *in vivo* potential. On the other hand, it would also be interesting to explore the incorporation of organic photothermal agents in the developed Thiol-Maleimide implantable hydrogels.

CRediT authorship contribution statement

Francisco J.P. Costa: Investigation, Formal analysis, Writing – original draft. **Micaela Nave:** Investigation. **Rita Lima-Sousa:** Investigation, Supervision, Writing – review & editing. **Cátia G. Alves:** Investigation. **Bruna L. Melo:** Investigation. **Ilídio J. Correia:** Project administration, Funding acquisition, Supervision, Writing – review & editing. **Duarte de Melo-Diogo:** Conceptualization, Investigation, Funding acquisition, Supervision, Writing – review & editing.

Declaration of Competing Interest

The authors declare that they have no known competing financial interests or personal relationships that could have appeared to influence the work reported in this paper.

Data availability

Data will be made available on request.

Acknowledgements

This work was developed within the scope of the CICS-UBI projects UIDB/00709/2020 and UIDP/00709/2020, financed by national funds through the Portuguese Foundation for Science and Technology/MCTES. The funding form POCI-01-0145-FEDER-031462, PTDC/BTABTA/0696/2020 and 2022.06320.PTDC is also acknowledged. Duarte de Melo-Diogo acknowledges FCT for the financial support given through a Junior Researcher contract (2021.00590.CEECIND). Cátia G. Alves, Rita Lima-Sousa and Bruna L. Melo acknowledge funding from individual PhD fellowships from FCT (SFRH/BD/145386/2019, SFRH/BD/144922/2019 and 2021.06044.BD).

Appendix A. Supplementary material

Supplementary data to this article can be found online at https://doi.org/10.1016/j.ijpharm.2023.122713.

References

Ahmadi, F., Oveisi, Z., Samani, S.M., Amoozgar, Z., 2015. Chitosan based hydrogels: characteristics and pharmaceutical applications. Res. Pharm. Sci. 10 (1), 1–16.

Alavi, M., Hamidi, M., 2019. Passive and active targeting in cancer therapy by liposomes and lipid nanoparticles. Drug Metabol. Personal. Therapy 34 (1). https://doi.org/10.1515/dmpt-2018-0032.

Askari, E., Seyfoori, A., Amereh, M., Gharaie, S.S., Ghazali, H.S., Ghazali, Z.S., Khunjush, B., Akbari, M., 2020. Stimuli-responsive hydrogels for local post-surgical drug delivery. Gels 6 (2), 14. https://doi.org/10.3390/gels6020014.

Attia, M.F., Anton, N., Wallyn, J., Omran, Z., Vandamme, T.F., 2019. An overview of active and passive targeting strategies to improve the nanocarriers efficiency to tumour sites. J. Pharm. Pharmacol. 71 (8), 1185–1198. https://doi.org/10.1111/jphp.13098.

Bashir, S., Hina, M., Iqbal, J., Rajpar, A.H., Mujtaba, M.A., Alghamdi, N.A., Wageh, S., Ramesh, K., Ramesh, S., 2020. Fundamental concepts of hydrogels: synthesis, properties, and their applications. Polymers 12 (11), 2702. https://doi.org/10.3390/polym12112702.

Bertrand, N., Wu, J., Xu, X., Kamaly, N., Farokhzad, O.C., 2014. Cancer nanotechnology: the impact of passive and active targeting in the era of modern cancer biology. Adv. Drug Deliv. Rev. 66, 2–25. https://doi.org/10.1016/j.addr.2013.11.009.

Bustamante-Torres, M., Romero-Fierro, D., Arcentales-Vera, B., Palomino, K., Magaña, H., Bucio, E., 2021. Hydrogels classification according to the physical or chemical interactions and as stimuli-sensitive materials. Gels 7 (4), 182. https://doi.org/10.3390/gels7040182.

Darling, N.J., Hung, Y.-S., Sharma, S., Segura, T., 2016. Controlling the kinetics of thiol-maleimide Michael-type addition gelation kinetics for the generation of homogenous poly(ethylene glycol) hydrogels. Biomaterials 101, 199–206. https://doi.org/10.1016/j.biomaterials.2016.05.053.

Deng, Y., Ren, J., Chen, G., Li, G., Wu, X., Wang, G., Gu, G., Li, J., 2017. Injectable in situ cross-linking chitosan-hyaluronic acid based hydrogels for abdominal tissue regeneration. Sci. Rep. 7 (1) https://doi.org/10.1038/s41598-017-02962-z.

Dhaliwal, A., Zheng, G., 2019. Improving accessibility of EPR-insensitive tumor phenotypes using EPR-adaptive strategies: designing a new perspective in nanomedicine delivery. Theranostics. 9 (26), 8091–8108. https://doi.org/10.7150/thno.37204.

Dimatteo, R., Darling, N.J., Segura, T., 2018. In situ forming injectable hydrogels for drug delivery and wound repair. Adv. Drug Deliv. Rev. 127, 167–184. https://doi.org/10.1016/j.addr.2018.03.007.

El-Sayed, N.S., Shirazi, A.N., El-Meligy, M.G., El-Ziaty, A.K., Nagieb, Z.A., Parang, K., Tiwari, R.K., 2016. Design, synthesis, and evaluation of chitosan conjugated GGRGDSK peptides as a cancer cell-targeting molecular transporter. Int. J. Biol. Macromol. 87, 611–622. https://doi.org/10.1016/j.ijbiomac.2016.03.020.

Ewald, J., Blankenburg, J., Worm, M., Besch, L., Unger, R.E., Tremel, W., Frey, H., Pohlit, H., 2020. Acid-cleavable poly(ethylene glycol) hydrogels displaying protein release at pH 5. Chem. –Euro. J. 26 (13), 2947–2953. https://doi.org/10.1002/chem.201905310.

Ganguly, S., Margel, S., 2021. Design of magnetic hydrogels for hyperthermia and drug delivery. Polymers 13 (23), 4259. https://doi.org/10.3390/polym13234259.

Gaspar, V.M., Sousa, F., Queiroz, J.A., Correia, I.J., 2010. Formulation of chitosan–TPP–pDNA nanocapsules for gene therapy applications. Nanotechnology 22 (1), 015101. https://doi.org/10.1088/0957-4484/22/1/015101.

Guaresti, O., Basasoro, S., González, K., Eceiza, A., Gabilondo, N., 2019. In situ cross–linked chitosan hydrogels via Michael addition reaction based on water–soluble thiol–maleimide precursors. Eur. Polym. J. 119, 376–384. https://doi.org/10.1016/j.eurpolymj.2019.08.009.

Hamilton, M., Harrington, S., Dhar, P., Stehno-Bittel, L., 2021. Hyaluronic acid hydrogel microspheres for slow release stem cell delivery. ACS Biomater. Sci. Eng. 7 (8), 3754–3763. https://doi.org/10.1021/acsbiomaterials.1c00658.

He, J., Chen, G., Zhao, P., Ou, C., 2021. Near-infrared light-controllable bufalin delivery from a black phosphorus-hybrid supramolecular hydrogel for synergistic photothermal-chemo tumor therapy. Nano Res. 14 (11), 3988–3998. https://doi.org/10.1007/s12274-021-3325-z.

Hoare, T.R., Kohane, D.S., 2008. Hydrogels in drug delivery: progress and challenges. Polymer 49 (8), 1993–2007. https://doi.org/10.1016/j.polymer.2008.01.027.

Hu, M., Yang, J., Xu, J., 2021. Structural and biological investigation of chitosan/hyaluronic acid with silanized-hydroxypropyl methylcellulose as an injectable reinforced interpenetrating network hydrogel for cartilage tissue engineering. Drug Deliv. 28 (1), 607–619. https://doi.org/10.1080/10717544.2021.1895906.

Huang, X., Jain, P.K., El-Sayed, I.H., El-Sayed, M.A., 2006. Determination of the minimum temperature required for selective photothermal destruction of cancer cells with the use of immunotargeted gold nanoparticles. Photochem. Photobiol. 82 (2), 412. https://doi.org/10.1562/2005-12-14-ra-754.

Jansen, L.E., Negrón-Piñeiro, L.J., Galarza, S., Peyton, S.R., 2018. Control of thiol-maleimide reaction kinetics in PEG hydrogel networks. Acta Biomater. 70, 120–128. https://doi.org/10.1016/j.actbio.2018.01.043.

Kearney, C.J., Mooney, D.J., 2013. Macroscale delivery systems for molecular and cellular payloads. Nat. Mater. 12 (11), 1004–1017. https://doi.org/10.1038/nmat3758.

Kumari, A., Singla, R., Guliani, A., Yadav, S.K., 2014. Nanoencapsulation for drug delivery. Excli. J. 13, 265–286.

Li, J., Mooney, D.J., 2016. Designing hydrogels for controlled drug delivery. Nat. Rev. Mater. 1 (12), 16071. https://doi.org/10.1038/natrevmats.2016.71.

Lima-Sousa, R., Alves, C.G., Melo, B.L., Moreira, A.F., Mendonça, A.G., Correia, I.J., de Melo-Diogo, D., 2021. Poly(2-ethyl-2-oxazoline) functionalized reduced graphene oxide: optimization of the reduction process using dopamine and application in cancer photothermal therapy. Mater. Sci. Eng. C 130, 112468. https://doi.org/10.1016/j.msec.2021.112468.

Lima-Sousa, R., de Melo-Diogo, D., Alves, C.G., Cabral, C.S.D., Miguel, S.P., Mendonça, A.G., Correia, I.J., 2020. Injectable in situ forming thermo-responsive graphene based hydrogels for cancer chemo-photothermal therapy and NIR light-enhanced antibacterial applications. Mater. Sci. Eng. C Mater. Biol. Appl. 117, 111294 https://doi.org/10.1016/j.msec.2020.111294.

Lima-Sousa, R., de Melo-Diogo, D., Alves, C.G., Costa, E.C., Ferreira, P., Louro, R.O., Correia, I.J., 2018. Hyaluronic acid functionalized green reduced graphene oxide for targeted cancer photothermal therapy. Carbohydr. Polym. 200, 93–99. https://doi.org/10.1016/j.carbpol.2018.07.066.

Liu, Z., Fan, L., Xiao, H., Cao, C., 2016. A multiple covalent crosslinked soft hydrogel for bioseparation. Chem. Commun. 52 (15), 3247–3250. https://doi.org/10.1039/c5cc09944g.

Lupu, A., Rosca, I., Gradinaru, V.R., Bercea, M., 2023. Temperature induced gelation and antimicrobial properties of pluronic F127 based systems. Polymers 15 (2), 355. https://doi.org/10.3390/polym15020355.

Maeda, H., 2015. Toward a full understanding of the EPR effect in primary and metastatic tumors as well as issues related to its heterogeneity. Adv. Drug Deliv. Rev. 91, 3–6. https://doi.org/10.1016/j.addr.2015.01.002.

Mather, B.D., Viswanathan, K., Miller, K.M., Long, T.E., 2006. Michael addition reactions in macromolecular design for emerging technologies. Prog. Polym. Sci. 31 (5), 487–531. https://doi.org/10.1016/j.progpolymsci.2006.03.001.

Matsumoto, M., Udomsinprasert, W., Laengee, P., Honsawek, S., Patarakul, K., Chirachanchai, S., 2016. A water-based chitosan-maleimide precursor for bioconjugation: an example of a rapid pathway for an in situ injectable adhesive gel. Macromol. Rapid Commun. 37 (19), 1618–1622. https://doi.org/10.1002/marc.201600257.

Melo, B.L., Lima-Sousa, R., Alves, C.G., Ferreira, P., Moreira, A.F., Correia, I.J., Melo-Diogo, D.d., 2021. Sulfobetaine methacrylate-albumin-coated graphene oxide incorporating IR780 for enhanced breast cancer phototherapy. Nanomedicine 16 (6), 453–464. https://doi.org/10.2217/nnm-2020-0460.

Melo, B.L., Lima-Sousa, R., Alves, C.G., Moreira, A.F., Correia, I.J., de Melo-Diogo, D., 2022. Chitosan-based injectable in situ forming hydrogels containing dopamine-reduced graphene oxide and resveratrol for breast cancer chemo-photothermal therapy. Biochem. Eng. J. 185, 108529 https://doi.org/10.1016/j.bej.2022.108529.

Mitchell, M.J., Billingsley, M.M., Haley, R.M., Wechsler, M.E., Peppas, N.A., Langer, R., 2021. Engineering precision nanoparticles for drug delivery. Nat. Rev. Drug Discov. 20 (2), 101–124. https://doi.org/10.1038/s41573-020-0090-8.

Mó, I., Alves, C.G., De Melo-Diogo, D., Lima-Sousa, R., Correia, I.J., 2020. Assessing the combinatorial chemo-photothermal therapy mediated by sulfobetaine methacrylate-functionalized nanoparticles in 2D and 3D in vitro cancer models. Biotechnol. J. 15 (12), 2000219. https://doi.org/10.1002/biot.202000219.

Mondal, A., Gebeyehu, A., Miranda, M., Bahadur, D., Patel, N., Ramakrishnan, S., Rishi, A.K., Singh, M., 2019. Characterization and printability of Sodium alginate-Gelatin hydrogel for bioprinting NSCLC co-culture. Sci. Rep. 9 (1), 19914. https://doi.org/10.1038/s41598-019-55034-9.

Moreira, A.F., Rodrigues, C.F., Jacinto, T.A., Miguel, S.P., Costa, E.C., Correia, I.J., 2019. Microneedle-based delivery devices for cancer therapy: a review. Pharmacol. Res. 148, 104438 https://doi.org/10.1016/j.phrs.2019.104438.

Mura, S., Nicolas, J., Couvreur, P., 2013. Stimuli-responsive nanocarriers for drug delivery. Nat. Mater. 12 (11), 991–1003. https://doi.org/10.1038/nmat3776.

Nair, D.P., Podgórski, M., Chatani, S., Gong, T., Xi, W., Fenoli, C.R., Bowman, C.N., 2014. The Thiol-Michael addition click reaction: a powerful and widely used tool in materials chemistry. Chem. Mater. 26 (1), 724–744. https://doi.org/10.1021/cm402180t.

Olaru, A.-M., Marin, L., Morariu, S., Pricope, G., Pinteala, M., Tartau-Mititelu, L., 2018. Biocompatible chitosan based hydrogels for potential application in local tumour therapy. Carbohydr. Polym. 179, 59–70. https://doi.org/10.1016/j.carbpol.2017.09.066.

Ozcelik, B., 2016. 7 - Degradable hydrogel systems for biomedical applications. In: Poole-Warren, L., Martens, P., Green, R. (Eds.), Biosynthetic Polymers for Medical Applications . Woodhead Publishing. pp. 173–188. doi: 10.1016/B978-1-78242-105-4.00007-9.

Parhi, R., 2017. Cross-linked hydrogel for pharmaceutical applications: a review. Adv. Pharm. Bull. 7 (4), 515–530. https://doi.org/10.15171/apb.2017.064.

Park, S.H., Seo, J.Y., Park, J.Y., Ji, Y.B., Kim, K., Choi, H.S., Choi, S., Kim, J.H., Min, B.H., Kim, M.S., 2019. An injectable, click-crosslinked, cytomodulin-modified hyaluronic acid hydrogel for cartilage tissue engineering. NPG Asia Mater. 11 (1) https://doi.org/10.1038/s41427-019-0130-1.

Pearce, A.K., O'Reilly, R.K., 2019. Insights into active targeting of nanoparticles in drug delivery: advances in clinical studies and design considerations for cancer nanomedicine. Bioconjug. Chem. 30 (9), 2300–2311. https://doi.org/10.1021/acs.bioconjchem.9b00456.

Pereira de Sousa, I., Suchaoin, W., Zupančič, O., Leichner, C., Bernkop-Schnürch, A., 2016. Totally S-protected hyaluronic acid: evaluation of stability and mucoadhesive properties as liquid dosage form. Carbohydr. Polym. 152, 632–638. https://doi.org/10.1016/j.carbpol.2016.06.051.

Rosenblum, D., Joshi, N., Tao, W., Karp, J.M., Peer, D., 2018. Progress and challenges towards targeted delivery of cancer therapeutics. Nat. Commun. 9 (1) https://doi.org/10.1038/s41467-018-03705-y.

Sabino, I.J., Lima-Sousa, R., Alves, C.G., Melo, B.L., Moreira, A.F., Correia, I.J., de Melo-Diogo, D., 2021. Injectable in situ forming hydrogels incorporating dual-nanoparticles for chemo-photothermal therapy of breast cancer cells. Int. J. Pharm. 600, 120510 https://doi.org/10.1016/j.ijpharm.2021.120510.

Seo, J.W., Shin, S.R., Lee, M.Y., Cha, J.M., Min, K.H., Lee, S.C., Shin, S.Y., Bae, H., 2021. Injectable hydrogel derived from chitosan with tunable mechanical properties via hybrid-crosslinking system. Carbohydr. Polym. 251, 117036 https://doi.org/10.1016/j.carbpol.2020.117036.

Shanmugam, V., Selvakumar, S., Yeh, C.-S., 2014. Near-infrared light-responsive nanomaterials in cancer therapeutics. Chem. Soc. Rev. 43 (17), 6254–6287. https://doi.org/10.1039/c4cs00011k.

Shariatinia, Z., Jalali, A.M., 2018. Chitosan-based hydrogels: preparation, properties and applications. Int. J. Biol. Macromol. 115, 194–220. https://doi.org/10.1016/j.ijbiomac.2018.04.034.

Sheth, S., Barnard, E., Hyatt, B., Rathinam, M., Zustiak, S.P., 2019. Predicting drug release from degradable hydrogels using fluorescence correlation spectroscopy and mathematical modeling. Front. Bioeng. Biotechnol. 7, 410. https://doi.org/10.3389/fbioe.2019.00410.

Shtenberg, Y., Goldfeder, M., Schroeder, A., Bianco-Peled, H., 2017. Alginate modified with maleimide-terminated PEG as drug carriers with enhanced mucoadhesion. Carbohydr. Polym. 175, 337–346. https://doi.org/10.1016/j.carbpol.2017.07.076.

Sriraman, S.K., Aryasomayajula, B., Torchilin, V.P., 2014. Barriers to drug delivery in solid tumors. Tissue Barrier 2 (3), e29528. https://doi.org/10.4161/tisb.29528.

Sun, Z., Song, C., Wang, C., Hu, Y., Wu, J., 2020. Hydrogel-based controlled drug delivery for cancer treatment: a review. Mol. Pharm. 17 (2), 373–391. https://doi.org/10.1021/acs.molpharmaceut.9b01020.

Trombino, S., Servidio, C., Curcio, F., Cassano, R., 2019. Strategies for hyaluronic acid-based hydrogel design in drug delivery. Pharmaceutics. 11 (8), 407. https://doi.org/10.3390/pharmaceutics11080407.

Wang, Y., Zhang, S., Benoit, D.S.W., 2018. Degradable poly(ethylene glycol) (PEG)-based hydrogels for spatiotemporal control of siRNA/nanoparticle delivery. J Control Release. 287, 58–66. https://doi.org/10.1016/j.jconrel.2018.08.002.

Wilhelm, S., Tavares, A.J., Dai, Q., Ohta, S., Audet, J., Dvorak, H.F., Chan, W.C.W., 2016. Analysis of nanoparticle delivery to tumours. Nat. Rev. Mater. 1 (5), 16014. https://doi.org/10.1038/natrevmats.2016.14.

Wu, Y., Chen, F., Huang, N., Li, J., Wu, C., Tan, B., Liu, Y., Li, L., Yang, C., Shao, D., Liao, J., 2021. Near-infrared light-responsive hybrid hydrogels for the synergistic chemo-photothermal therapy of oral cancer. Nanoscale 13 (40), 17168–17182. https://doi.org/10.1039/d1nr04625j.

Xie, R., Chen, Y.-C., Zhao, Y., Yodsanit, N., Wang, Y., Yamamoto, N., Yamanouchi, D., Gong, S., 2021. Injectable hydrogel capable of in situ covalent crosslinking for permanent embolization. ACS Appl. Mater. Interfaces 13 (48), 56988–56999. https://doi.org/10.1021/acsami.1c18250.

Yang, X., Gao, L., Wei, Y., Tan, B., Wu, Y., Yi, C., Liao, J., 2021. Photothermal hydrogel platform for prevention of post-surgical tumor recurrence and improving breast reconstruction. J. Nanobiotechnol. 19 (1) https://doi.org/10.1186/s12951-021-01041-w.

Zhang, H., Zhang, M., Zhang, X., Gao, Y., Ma, Y., Chen, H., Wan, J., Li, C., Wang, F., Sun, X., 2022a. Enhanced postoperative cancer therapy by iron-based hydrogels. Biomater. Res. 26 (1) https://doi.org/10.1186/s40824-022-00268-4.

Zhang, J., Lin, Y., Lin, Z., Wei, Q., Qian, J., Ruan, R., Jiang, X., Hou, L., Song, J., Ding, J., Yang, H., 2022b. Stimuli-responsive nanoparticles for controlled drug delivery in synergistic cancer immunotherapy. Adv. Sci. 9 (5), 2103444. https://doi.org/10.1002/advs.202103444.

Zhang, Y., Cao, J., Yuan, Z., 2020. Strategies and challenges to improve the performance of tumor-associated active targeting. J. Mater. Chem. B 8 (18), 3959–3971. https://doi.org/10.1039/d0tb00289e.

Zhou, M., Zuo, Q., Huang, Y., Li, L., 2022. Immunogenic hydrogel toolkit disturbing residual tumor “seeds” and pre-metastatic “soil” for inhibition of postoperative tumor recurrence and metastasis. Acta Pharm. Sin. B 12 (8), 3383–3397. https://doi.org/10.1016/j.apsb.2022.02.017.